

# Covalent Lysozyme Immobilization on Enzymatic Cellulose Nanocrystals

Laura Spagnuolo,<sup>[a, b]</sup> Laura Micheli,<sup>[c]</sup> Alain Dufresne,<sup>[d]</sup> Davide Beneventi,<sup>[d]</sup> and  
Alessandra Operamolla\*<sup>[a, b]</sup>

Nanostructured materials represent promising substrates for biocatalyst immobilization and activation. Cellulose nanocrystals (CNCs), accessible from waste and/or renewable sources, are sustainable and biodegradable, show high specific surface area for anchoring a high number of enzymatic units, and high thermal and mechanical stability. In this work, we present a holistic enzyme-based approach to functional antibacterial materials by bioconjugation between the lysozyme from chicken egg white and enzymatic cellulose nanocrystals. The neutral CNCs were prepared by endoglucanase hydrolysis from Avicel. We explore the covalent immobilization of lysozyme on

enzymatic CNCs and on their TEMPO oxidized derivatives (TO-CNCs), comparing immobilization yields, material properties, and enzymatic activities. The materials were characterized by X-ray diffractometry (XRD), attenuated total reflectance Fourier Transform infrared spectroscopy (ATR-FTIR), bicinchoninic acid (BCA) assay, field-emission scanning electron microscopy (FE-SEM) and dynamic light scattering (DLS). We demonstrate the higher overall efficiency of the immobilization process carried out on TO-CNCs, based on the success of covalent bonding and on the stability of the isolated bioconjugates.

## Introduction

In recent decades, synthetic polymers have caused serious environmental problems such as the widespread accumulation of microplastics and contribution to global climate change, with their unfavorable environmental footprint.<sup>[1]</sup> For this reason, many researchers have focused on the search for bio-based alternatives and the research world is moving from petroleum-based polymers to sustainable and renewable substitutes. In this respect, biomass can play an important role as it can be used as a source of a wide range of bio-products. Among these, cellulose has many interesting features, including renewability, edibility, biodegradability, and low cost.<sup>[2]</sup> Furthermore, it is the most abundant organic polymer in nature. Cellulose is a linear polysaccharide consisting of  $\beta$ -D-

glucopyranose units linked to each other by 1,4-O-glycosidic bridges.<sup>[3]</sup>

Nanocellulose, a versatile cellulose nanomaterial, has attracted much attention for its potential applications in various fields.<sup>[4,5]</sup> In addition, the aspect of sustainability arising from the use of enzymes in nanocellulose production further enhances its appeal.<sup>[6–9]</sup> Enzymatic processes, indeed, reduce environmental impact compared to aggressive chemical treatments,<sup>[10]</sup> and are highly specific allowing precise control on size and morphology of nanocellulose.<sup>[11]</sup>


This work aims to explore the intersection between the use of nanocellulose as an antibacterial agent and the enhancement of its antibacterial properties by bioconjugation with a specific enzyme, aiming at defining a holistic enzymatic approach to antibacterial materials based on mechano-enzymatic nanocellulose/enzymes bioconjugates.<sup>[12,13]</sup> The antibacterial activity has immense potential for applications in wound dressings, antimicrobial coatings, and food packaging, where control of bacterial contamination is critical.<sup>[14]</sup> Previous studies have shown that nanocellulose possesses inherent antibacterial properties attributed to its nanostructure and surface chemistry.<sup>[15]</sup> These properties enable nanocellulose to inhibit the growth of various bacteria, including Gram-positive and Gram-negative strains. Enzymes are widely used in food, medicine, energy, and other fields due to their high catalytic efficiency.<sup>[16]</sup> Immobilization can solve obstacles as instability, difficulty in separation, and lack of control over activity, by improving the properties of biocatalysts.<sup>[17,18]</sup> Applications of immobilized enzymes include their use in the biomedical field for the preparation of new drugs, such as immobilized L-asparaginase, which is used for the treatment of leukaemia, for the formulation of detergents to remove lipid stains from cold textiles or even as ingredient in cosmetics.<sup>[19]</sup>


[a] L. Spagnuolo, A. Operamolla  
Dipartimento di Chimica e Chimica Industriale, Università di Pisa, via  
Giuseppe Moruzzi 13, I-56124, Pisa, Italy  
E-mail: alessandra.operamolla@unipi.it

[b] L. Spagnuolo, A. Operamolla  
Interuniversity Consortium of Chemical Reactivity and Catalysis (CIRCC), Via  
Celso Ulpiani 27, I-70126, Bari, Italy

[c] L. Micheli  
Dipartimento di Scienze e Tecnologie Chimiche, Università degli Studi di  
Roma Tor Vergata, via della Ricerca Scientifica, 00133 Roma, Italy.

[d] A. Dufresne, D. Beneventi  
Université Grenoble Alpes, CNRS, Grenoble INP, LGP2, F-38000 Grenoble,  
France.

 Supporting information for this article is available on the WWW under  
<https://doi.org/10.1002/chem.202402171>

 © 2024 The Author(s). Chemistry - A European Journal published by Wiley-VCH GmbH. This is an open access article under the terms of the Creative Commons Attribution Non-Commercial NoDerivs License, which permits use and distribution in any medium, provided the original work is properly cited, the use is non-commercial and no modifications or adaptations are made.

There are several new technologies and methods in the field of enzyme immobilization such as immobilization on nanomaterials, which, having a high surface area, allow a high number of protein units to be bound. Cellulose nanocrystals (CNCs) are ideal carriers due to their biocompatible nature, large surface area, high specific strength and high dispersibility in aqueous medium.<sup>[20–26]</sup> Furthermore, CNCs are safer than other nanomaterials and are non-toxic to microvascular endothelial cells in the human brain.<sup>[27,28]</sup> This makes the biocatalyst immobilized on nanocellulose more respectful for the health and the environment. CNCs are presently the focus of research in the biocatalysis field, with some enzymes successfully immobilized onto their surface, opening doors to innovative applications in green chemistry and biotechnology.<sup>[29–33]</sup>

Considering the above-described scenario, in this paper we present a fully enzymatic strategy to prepare modified cellulose nanocrystals with antibacterial properties by covalent immobilization. CNCs produced by enzymatic hydrolysis<sup>[12]</sup> are the ideal substrate for the covalent immobilization of biocatalysts. Enzymatic CNCs are explored as substrates for immobilization experiments of lysozyme from chicken's egg white.<sup>[34]</sup> The selected lysozyme (EC 235–747-3) has a molecular weight of ~14.4 kDa. Its relatively small size facilitates its movement across cellular barriers and contributes to its versatility in various biological and industrial applications. It is composed of 129 amino acid residues.<sup>[35]</sup> Its primary structure includes a combination of polar, nonpolar, acidic, and basic amino acids, contributing to its overall structure and function. The selected enzyme displays six lysine residues, seven aspartic acid and two glutamic acid residues, useful for covalent immobilization. Lysozyme adopts a compact globular structure, stabilized by disulfide bonds between cysteine residues. Its tertiary structure consists of a predominantly  $\alpha$ -helical and  $\beta$ -sheet arrangement, forming a catalytic cleft where substrate binding and enzymatic activity occur. The isoelectric point of lysozyme falls at pH 11.35.<sup>[36]</sup>

Using lysozyme from chicken egg white offers a notable advantage due to its abundance, cost-effectiveness, and stability. It is used in various applications, such as food preservation and pharmaceuticals, and its antimicrobial properties contribute to enhancing product safety and shelf life.<sup>[36,37]</sup> Additionally, its biocompatibility makes it suitable for use in various industries without adverse effects. Lysozyme exhibits hydrolytic activity against the  $\beta$ -1,4-glycosidic bonds present in the peptidoglycan layer of bacterial cell walls. This activity leads to bacterial cell lysis and is a key component of the innate immune response in organisms. Lysozyme demonstrates robust thermal stability,<sup>[38]</sup> retaining its enzymatic activity over a wide range of temperatures. This characteristic extends its applications to food processing since it can withstand heat treatments without losing efficacy.<sup>[39]</sup> These properties have recently evidenced the great potential of lysozyme as an antibacterial agent.<sup>[40]</sup>

Herein, we carry out an in-depth investigation on the best strategy to carry out the covalent bioconjugation, by describing different immobilization strategies.

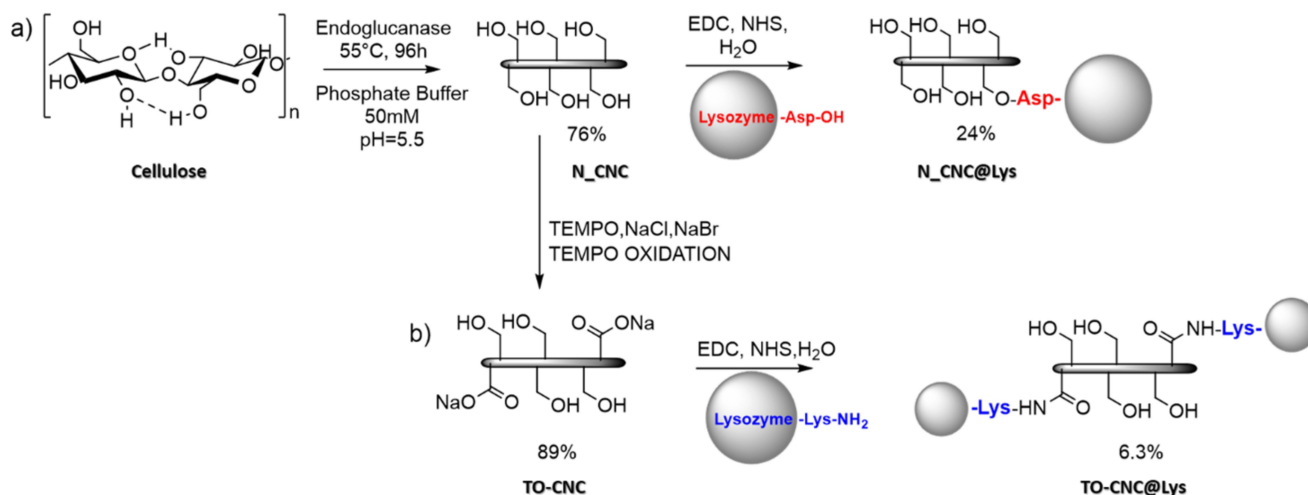
## Results and Discussion

### Immobilization Experiments

Before performing a covalent bioconjugation between lysozyme and the nanocrystals, we first investigated the activity of lysozyme by a kinetic test (Figures S1) and the possible nonspecific immobilization. Enzymatic neutral cellulose nanocrystals (N\_CNCs) were prepared from Avicel in 76% yield following our protocol,<sup>[12]</sup> exploiting endoglucanase from *Aspergillus niger* for the hydrolysis and pre-treatment of the cellulose-rich starting material by low frequency ball milling. Sulfated cellulose nanocrystals (S\_CNCs), instead, were prepared by sulfuric acid hydrolysis.<sup>[41]</sup> S\_CNCs are considered a benchmark in the field of nanocellulose. Most of the work on enzymes immobilization carried out by others was performed on sulfated CNCs.<sup>[29–33]</sup>

The nonspecific immobilization is based on weak interactions (hydrogen bonding, hydrophobic interactions) in the case of N\_CNCs, while in the case of S\_CNCs, it can also entail ionic interactions between negatively charged sulfate groups on the surface of the nanocrystals and positively charged lysine residues on lysozyme, provided the working pH is lower than the enzyme isoelectric point. The process of immobilizing lysozyme on nanocrystals, whether they be S\_CNC or N\_CNC, involved incubating lysozyme and nanocrystals in 1:10 weight ratio at a slightly alkaline pH of 8.0 and room temperature. This step is pivotal as it sets the stage for the interaction between the lysozyme molecules and the nanocrystals, promoting their immobilization. The immobilization pH was selected after a thorough examination of the stability of lysozyme at various pH values. The lysozyme pH stability plot, with the conditions experimented, is reported in the Supporting Information in Figure S2. The key purification step was a dialysis carried out in membranes with a Mw cut of 15,000 Da to remove excess enzyme. Although the immobilization was successful, as judged from ATR-FTIR and activity tests (Figures S3–S5), the non-specifically immobilized lysozyme on S\_CNCs and N\_CNCs lacked the necessary stability over time, rapidly losing the biocatalytic activity within few days.

This prompted us to move to a more robust approach, like covalent immobilization. The most straightforward way was performing the covalent immobilization reaction between the surface -OH groups of N\_CNCs and the -COOH of the Asp and Glu residues on the enzyme in the presence of EDC (1-ethyl-3-(3-dimethylaminopropyl)carbodiimide) and N-hydroxysuccinimide (NHS) in water (Scheme 1a). The lysozyme to CNCs weight ratio was increased to 2:1 as reported in a previous procedure.<sup>[42]</sup> However, despite the successful formation of enzyme/nanocrystal biohybrids, the catalytic activity of the immobilized lysozyme on N\_CNCs was significantly reduced after one week, as discussed later. This could be either attributed to unfavourable conformational changes induced by the immobilization process, or to an inefficient covalent binding, due to the low dispersibility of N\_CNCs in the reaction medium, which prevents the formation of a relevant number of covalent linkages between the N\_CNCs and



Scheme 1. Covalent immobilization of lysozyme: (a) on N\_CNCs and (b) on TO-CNC.

lysozyme. This highlighted the need to change the immobilization strategy to achieve the desired biocatalytic performance.

Considering the unsatisfactory results of the first bioconjugation approach, we decided to perform the covalent immobilization on TEMPO-oxidized enzymatic nanocrystals (TO-CNCs), which present surface carboxyl groups. These nanocrystals display increased dispersibility in water, as an effect of the surface charge introduced by the carboxylate anions formed at the immobilization pH. TO-CNCs were prepared from enzymatic N\_CNCs by following a previously published procedure.<sup>[43,44]</sup> During oxidation, N\_CNCs were dispersed in water at pH 11, and the reaction was performed using 15% NaClO<sub>aq</sub> as the oxidant and NaBr and 2,2,6,6-tetramethylpiperidine-1-oxylradical (TEMPO) as catalysts. TO-CNCs were purified by dialysis against deionized water and isolated in 89% yield. X-ray diffraction spectra (XRD, plots reported in Figure 1) acquired on both N\_CNCs and TO-CNCs showed that crystallinity of N\_CNC is 91% and crystallinity of TO-CNCs is 87%. Crystallinity of TO-CNCs and N\_CNCs was calculated by the Segal method.<sup>[45]</sup>

The bioconjugation with lysozyme was performed between the pending carboxyl groups of TO-CNCs and the lysine residues of the enzyme, exploiting again EDC and NHS chemistry, to facilitate the formation of stable amide bonds (Scheme 1b). The TO-CNCs, preactivated by mixing with EDC and NHS, were mixed in 10:1 weight ratio to the enzyme. The isolation of the biohybrid system was performed as described in the previous case.

### Characterization of the Bioconjugates

The characterization of the biohybrid systems involved various analytical techniques. These included attenuated total reflectance Fourier transform infrared spectroscopy (ATR-FTIR), the bicinchoninic acid (BCA) test to assess the loading of enzyme in the biohybrid systems, field emission-scanning electron

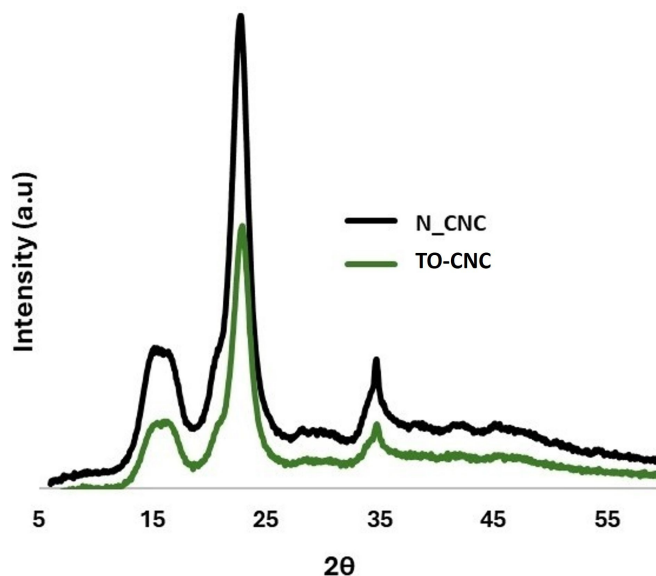
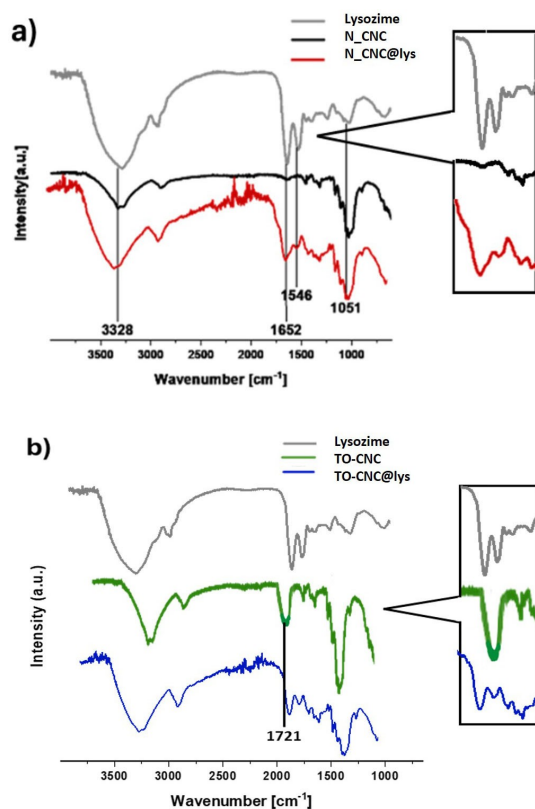


Figure 1. XRD spectra of N\_CNC (black trace) and TO-CNC (green trace).

microscopy (FE-SEM), dynamic light scattering (DLS) and  $\zeta$ -potential, and kinetic activity tests.

Figure 2a illustrates the ATR-FTIR spectra of lysozyme, N\_CNCs, and their bioconjugate N\_CNCs@lysozyme. In N\_CNCs, a significant peak, observed around 3328 cm<sup>-1</sup>, corresponds to the stretching vibrations of hydroxyl groups (OH). Another distinctive region in the spectrum, centered around 2900 cm<sup>-1</sup>, displays signals attributed to the stretching vibrations of aliphatic carbon-hydrogen bonds of the glycosidic ring (C-H). Furthermore, intense signals around 1050 cm<sup>-1</sup> are linked to stretching vibrations of carbon-oxygen bonds (C-O-C), prevalent in the glycosidic bonds of cellulose, highlighting the connectivity of glucose units through acetal bonds, whilst the 1646 cm<sup>-1</sup> peak evidences the presence of crystallized water in the nanocrystals.



**Figure 2.** ATR spectra: (a) In grey lysozyme; in black N\_CNC; in red N\_CNC@lysozyme; (b) In grey lysozyme; in green TO-CNC; in blue TO-CNC@lysozyme

Lysozyme shows in the ATR-FTIR spectrum the typical peaks corresponding to amide bonds ( $\sim 1650\text{ cm}^{-1}$  for C=O stretching, amide I band, and  $\sim 1550\text{ cm}^{-1}$  for N–H bending, amide II band), along with characteristic bands of amino acid side chains, such as aromatic C–H stretching ( $\sim 3000\text{--}3100\text{ cm}^{-1}$ ) and aliphatic C–H stretching ( $\sim 2800\text{--}3000\text{ cm}^{-1}$ ). The biohybrid system shows that the characteristic peaks corresponding to the amide bonds of lysozyme are shifted (amide I band from  $1650\text{ cm}^{-1}$  to  $1652\text{ cm}^{-1}$ , and amide II band from  $1550\text{ cm}^{-1}$  to  $1546\text{ cm}^{-1}$ ). A weak signal appears as a shoulder at  $1701\text{ cm}^{-1}$ , sign of the formation of ester bonds between the carboxyl groups of lysozyme residues and surface hydroxyl groups on cellulose nanocrystals. This spectrum suggests the efficacy of the immobilization process. However, the low intensity of the ester bond observed in the ATR-FTIR of the sample and the broader amide bands appearing for the biohybrid demonstrated the presence not only of ester bonds between the nanocrystals and the protein, but also the possible formation of a cross-linked enzyme aggregate (CLEA)<sup>[46]</sup> of lysozyme through the enzyme self-reaction between activated aspartic/glutamic residues and lysines. This aspect was previously overlooked.<sup>[24]</sup>

Figure 2b illustrates the ATR-FTIR spectra of lysozyme, TO-CNCs, and their bioconjugate TO-CNCs@lysozyme. In TO-CNCs, a significant peak, observed around  $3354\text{ cm}^{-1}$ , corresponds to the stretching vibrations of hydroxyl groups with the contribu-

tion of the carboxyl units. Additionally, the distinctive peak associated with C=O stretching, appears at  $1721\text{ cm}^{-1}$ , reflecting the chemical modification of cellulose nanocrystals with the introduction of carboxyl functionalities. In the bioconjugate, the characteristic peaks corresponding to the amide bonds of lysozyme are shifted towards higher energies in the case of amide I band (from  $1650\text{ cm}^{-1}$  to  $1655\text{ cm}^{-1}$ ) and lower energies for amide II band (from  $1550\text{ cm}^{-1}$  to  $1540\text{ cm}^{-1}$ ), whilst the signal of C=O stretching of carboxyl moieties of TO-CNCs dramatically decreased in intensity, sign of their quantitative reaction with the lysozyme residues. This spectrum confirms the efficacy of the immobilization process.

The Bicinchoninic Acid (BCA) Test was performed on the immobilized systems dispersed in water to quantify the protein. A calibration curve ( $y = 0.084 + 0.0058x$ ,  $\text{RSD}\% = 1\%$ ,  $r^2 = 0.999$ ) was obtained using BSA (bovine serum albumin) as the reference standard (working range  $0\text{--}30\text{ }\mu\text{g/mL}$ , LOQ, quantification limit,  $2\text{ }\mu\text{g/mL}$ ) and was used to extrapolate the unknown concentration of the lysozyme immobilized on N\_CNC and TO-CNC (in order to fall in the working range of BCA assay, N\_CNC and TO-CNCs were diluted 1:10 v/v and 1:2 v/v, respectively). A reference containing CNCs was used to subtract from the measured absorbances the interference generated by the scattering of nanocrystals and their interaction with the test reagents through their available reducing termini.<sup>[47]</sup> The results, reported in Table 1, show that the process of immobilizing lysozyme on TO-CNCs was able to covalently immobilize 6.3% of the added lysozyme. Vice versa, immobilization on N\_CNCs, gave 24% overall yield. Therefore, judging from the BCA assay, N\_CNC@Lys had a higher enzyme content than TO-CNC@Lys. However, as previously described, the ATR-FTIR spectra indicate a not clearly covalent interaction between lysozyme and N\_CNCs.

FE-SEM analyses on N\_CNCs, TO-CNCs and the immobilized samples are shown in Figure 3. The FE-SEM micrograph of N\_CNCs revealed well-defined nanocrystals with consistent sizes, indicating successful extraction from Avicel. The average lengths of the nanocrystals were determined using IMAGE J software, yielding  $124 \pm 25\text{ nm}$  for N\_CNCs. TO-CNCs displayed a preserved rod-like morphology if compared to N\_CNCs. The micrograph corresponding to the sample N\_CNC@lys shows mixing of N\_CNC with a soft polymeric matrix. The efficient mixing with the protein is undoubtful, though big aggregates are found in the morphology. Effective polymer mixing is evident also in the TO-CNC@lys micrograph: the dispersion of TO-CNCs within the protein matrix this time shows a more homogeneous distribution and highlights their interpenetration. This visual confirmation underscores the compatibility

**Table 1.** Concentration of lysozyme extrapolated by BCA in the bioconjugates with nanocrystals.

Sample	Enzyme concentration [ $\mu\text{g/mL}$ ]	Enzyme immobilization yield
N_CNC@Lys	$4050 \pm 6$	24%
TO-CNC@lys	$1068 \pm 4$	6.3%



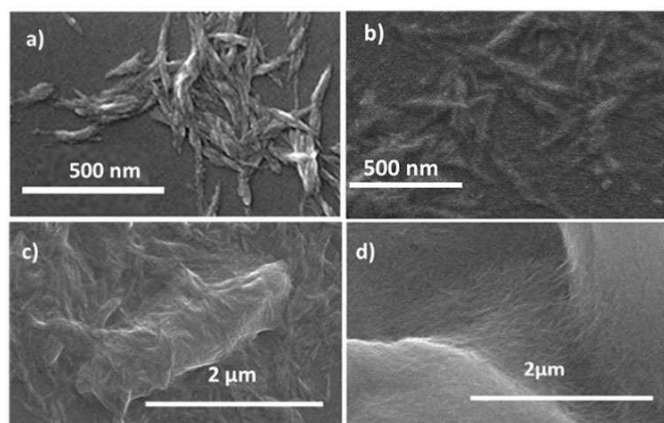


**Figure 3.** (a) FE-SEM images of enzymatic N\_CNC; (b) TO-CNC; (c) N\_CNC@lys; (d) TO-CNC@lys. The micrograph in 3 d was recorded on the lyophilized and rehydrated sample.

and interconnectivity achieved between the polymers, which is critical for improving material properties and performance. SEM images provide a qualitative assessment of blend uniformity, helping to evaluate the effectiveness of the immobilization experiments and supporting what inferred from ATR-FTIR.

The results of dynamic light scattering (DLS) and zeta potential measurements performed on water dispersions of N\_CNCs, TO-CNCs, TO-CNCs@lys, and N\_CNC@lys are depicted in the histograms presented in Figure 4 and summarized in Table 2. N\_CNCs exhibit a relatively narrow size distribution, evident from the low polydispersity index (PDI) of 0.4 (Table 2). The measured Z-average size of  $150 \pm 25$  nm aligns well with the length value observed in the FE-SEM micrograph, indicating uniformity and well-defined size profile of enzymatic CNCs.

Analyzing zeta potential histogram (Figure 4, bottom) reveals a slightly positive value of  $0.5 \pm 0.1$  mV for enzymatic N\_CNCs, indicating proximity to neutrality (Table 2). This minimal positive charge implies negligible repulsion between neutral N\_CNC particles, potentially leading to aggregation primarily influenced by van der Waals forces rather than electrostatic repulsion. TO-CNC displays a Z-average size around  $110 \pm 34$  nm and a zeta potential of approximately  $-20 \pm 2$  mV. N\_CNC@lys displays a Z-average size around  $200 \pm 34$  nm and a zeta potential of approximately  $-10 \pm 5$  mV, clear evidence of the appearance of a surface charge on N\_CNC@lys bioconjugates, due to the enzyme. The negative sign of total charge observed can be taken as a further confirmation of the lysine engagement in covalent bonds, supporting the formation of a CLEA. The size distribution plot derived from DLS measurements on N\_CNC@lys further supports the formation of a CLEA showing a bimodal size distribution (compare supporting information, Figures S6 for the plot and S7 for the peak deconvolution). TO-CNC@lys displays a Z-average size around  $400 \pm 87$  nm and a zeta potential of approximately  $-34 \pm 10$  mV. Again, the overall negative sign can be a consequence of lysine residues involvement in amide bonds.

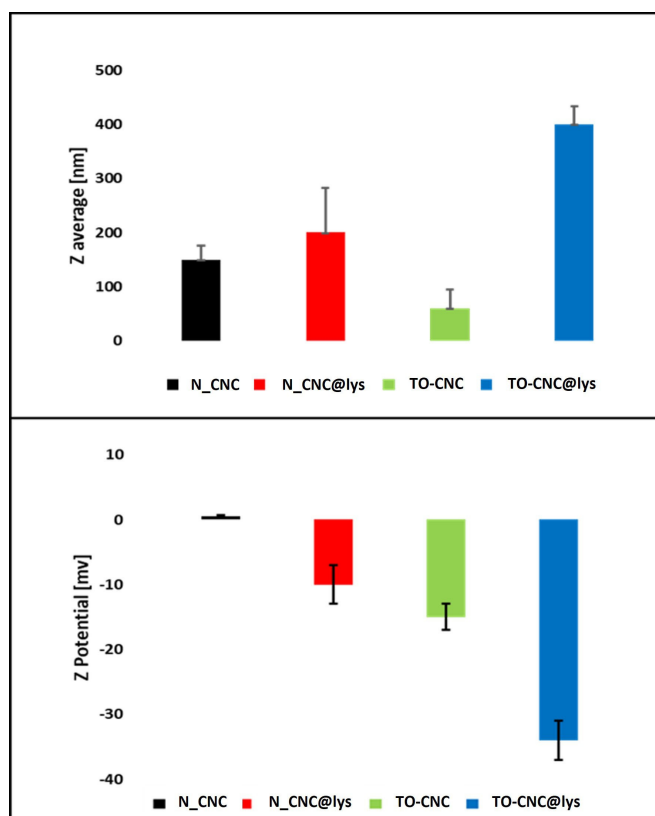


**Figure 4.** (a) Z-average histograms; (b) Z potential histograms.

**Table 2.** Characterization of CNC Samples: Polydispersity Index, Z-Average, and Zeta Potential.

Sample	Polydispersity index (PDI)	Z-Average [nm]	Zeta potential [mv]
N_CNC	0.4	$150 \pm 25$	$0.5 \pm 0.1$
TO-CNC	0.7	$110 \pm 34$	$-20 \pm 2$
N_CNC@lys	0.6	$200 \pm 34$	$-10 \pm 5$
TO-CNC@lys	0.6	$400 \pm 87$	$-34 \pm 10$

To verify the effective biocatalytic efficiency of the immobilized systems, *Micrococcus deykticus* activity tests, shown in Figure 5, were performed for each immobilized sample to confirm the preserved functionality of the enzyme. The N\_CNC@Lys sample displayed a fast kinetic within the first minute of the test. Considering the amount of immobilized lysozyme, the calculated enzymatic units per mL (U), collected for all samples in Table 3, were 1200. During the last 100 s of the test, the activity changed to a lower value of 133 U/mL. This behavior confirmed the co-presence of two different lysozyme immobilized systems in N\_CNC@Lys (a bioconjugate and a CLEA). Finally, the overall catalytic activity of N\_CNC@Lys disappeared within one week.

Conversely, TO-CNC@Lys displayed a slower digestion kinetic with a slight delay ( $\sim 50$  s) in optical density decrease and 233 U/mL total enzymatic activity. The delayed kinetic is

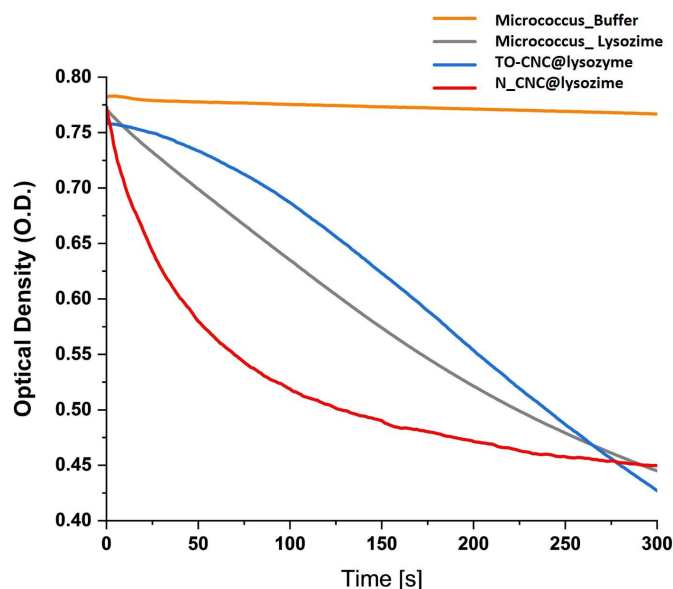


**Figure 5.** Lysozyme Activity Test results on N\_CNC@lys (red) and TO CNC@lys (blu). The plot shows the optical density of a suspension of *Micrococcus lysodeikticus* cells exposed to the samples. In orange *Micrococcus* in buffer; in grey of *Micrococcus*@lys.

Table 3. U* of immobilized samples.			
Sample	Time [s]	U/mL	U/mg immobilized Lys
N_CNC@lys	0–50	1200	296.3
	150–300	133	57.53
TO-CNC@Lys	0–300	233	218

\*Unit Definition (U): One unit of Lysozyme will produce a  $\Delta OD_{450}$  of 0.001 per minute at pH 6.24 at 25 °C using a suspension of *Micrococcus lysodeikticus* as substrate in a 2.6 mL reaction mixture.

in good agreement with the slow motion of the immobilized systems, whose size is determined by the combination of cellulose nanocrystals and covalently bonded protein. Furthermore, TO-CNCs@lysozyme bioconjugates are remarkably stable over time (after one month there was no appreciable activity decrement, Figure S8), a crucial advantage of the covalent immobilization approach involving carboxylated nanocrystals. This stability not only ensures the reliability of the approach but also improves its long-term effectiveness, providing a robust system for various applications. The behavior of the two samples was taken as a confirmation of the formation of a CLEA in the first case, with formation of a more soluble protein aggregate, even if with rapid deactivation for insufficient stabilization, and of the achievement of a true covalent immobilization on TO-CNCs.

## Conclusions

In conclusion, the covalent immobilization of lysozyme on cellulose nanocrystals reveals distinct advantages if the surface chemistry of the nanocrystals employed as substrate is taken

into consideration. The nonspecific immobilization, while relatively simple to achieve, lacks stability over time, compromising the performance and longevity of the immobilized enzyme. On the other hand, covalent immobilization using TEMPO-oxidized nanocrystals outperforms other immobilization strategies, demonstrating greater stability over time, attributed to the formation of strong covalent bonds between the enzyme and the nanocrystals. This stability ensures the preservation of enzyme activity and structural integrity, contributing to sustained performance and reusability of the immobilized lysozyme. Antibacterial properties towards other bacteria streams will be tested in the future to confirm the amenability of the new materials to be applied in the coating industry.

## Experimental Section

### Materials

Avicel® PH-101 (particle size ~50  $\mu\text{m}$ ), lysozyme from chicken egg white (EC235.747.3, lyophilized powder,  $\geq 90\%$  protein,  $\geq 40,000$  units/mg protein used for the immobilization experiments) and the lysozyme activity test kit were purchased from Sigma Aldrich,  $\text{Na}_2\text{HPO}_4 \cdot 2\text{H}_2\text{O}$  and  $\text{NaH}_2\text{PO}_4 \cdot 2\text{H}_2\text{O}$  were purchased from Fluka and cellulase (1,4-(1,3:1,4)- $\beta$ -D-Glucan 4-glucan-hydro-lase, EC3.2.1.2) from MP Biomedicals. EDC and NHS were purchased from Sigma Aldrich. S\_CNC was prepared according to Operamolla et al.<sup>[8]</sup> Dialysis tubing cellulose membrane to purify nanocrystals, avg. flat width 76 mm (3.0 in.) cut off 12,400 Da, was purchased from Sigma Aldrich. Tube-O-DIALYZER™ mini dialysis system with a Mw cut of 15 kDa to purify immobilized system was purchased from Biosciences.

### Production of N\_CNCs Via Enzymatic Hydrolysis

N\_CNCs were synthesized as reported by Spagnuolo et al.<sup>[12]</sup> Avicel pretreatment was performed using a ball miller (BM500, Anton Paar) loaded with 5 g of Avicel per 50 mL steel jars with one 2.5 cm steel ball each. The pretreatment involved a frequency of 3 Hz for the duration of 50 min. Then, ball milled Avicel (5.04 g) was mixed with 50 mL of 50 mM phosphate buffer at pH = 5.0 and homogenized using a tissue master. *Aspergillus niger* endoglucanase (28 mg, 253 mg, 516 mg, or 1 g) was added to the suspension, which was then incubated in an orbital shaker at 55 °C for 1 week. Subsequently, the reaction was heated to 95 °C for 15 min to deactivate the enzyme and centrifuged. The residue underwent washing with 0.1 M HCl and multiple washes with deionized  $\text{H}_2\text{O}$  until neutrality. After 24-h dialysis, the suspension was sonicated, centrifuged, and freeze-dried to obtain N\_CNCs in 76% yield. The crystallinity of the cellulose nanocrystals was judged from X-ray diffractograms.

### Synthesis of TO-CNC

1.03 g of enzymatic N\_CNCs were suspended in a 100 mL beaker in 60 mL deionized water using an immersion sonicator (constant duty cycle, 80 W power for 10 min). The suspension was transferred to a 250 mL three-neck round-bottom flask equipped with a dropping funnel and pH meter, and the pH of the dispersion was raised to 11 by adding the required amount of a 3.0 N NaOH aqueous solution. 115 mg of NaBr and 96 mg of TEMPO radical are

added. The system was stirred for an additional 10 min before beginning the dropwise addition of an aqueous solution of NaClO<sub>15</sub> % (25 mL, 49 mmol). During the reaction, the pH was constantly monitored and adjusted to 11 with the addition of NaOH 3.0 N. The addition stopped when following the addition of NaClO no decrease in pH was observed. Then, HCl 1.0 N was added until pH 3. The mixture was transferred to polypropylene tubes and centrifuged for 10 min at 4000 rpm. The solid material was re-suspended in deionized water (50 mL) and dialyzed with distilled water in a cellulose nitrate membrane with a molecular weight cutoff of 12 400 Da. The suspension was freeze-dried, and a white solid (0.913 g, 89 % yield) was obtained.

### Covalent Immobilization of Lysozyme on N\_CNCs

100 mg of lysozyme were dissolved in 5 ml of H<sub>2</sub>O. Then, 15 mg of EDC were added, and the mixture was gently mixed with orbital shaker for 30 min. This solution was added to a suspension of 50 mg of N\_CNC in 6 mL of Phosphate buffer at pH=8.0 100 mM, previously sonicated with a tip sonicator (0.6 cycle; 60 Amplitude). The mixture was allowed to react for 30 min at room temperature under orbital stirring. After 4 h, the mixture was centrifuged at 4000 rpm and 4 °C, the supernatant was discarded, and the residue purified by dialysis against deionized water with a mini dialysis kit.

### Covalent Immobilization of Lysozyme on TO-CNC

100 mg of TO-CNC were dissolved in 10 mL of water and sonicated with a tip sonicator (0.6 cycle; 60 Amplitude). 50 mg of EDC were dissolved in 1 mL of water and 50 mg of NHS were dissolved in 1 mL of water and these solutions were added to the TO-CNC suspension and let them react for 1 h. 10 mg of lysozyme were dissolved in 1 mL of phosphate buffer 100 mM at pH=8.0 and gently shaken for 5 min. Then, the lysozyme solution was added to the reaction medium. After 4 h, the mixture was centrifuged at 4000 rpm and 4 °C, the supernatant was discarded, and the residue purified by dialysis against deionized water with a mini dialysis kit.

### Elemental Analysis

The elemental analyses were carried out using a Vario Micro Cube CHNOS Elemental Analyzer, enabling quantitative, fully automated analysis of elements C, H, N, S, and O by combustion gas analysis. The instrument employs a thermal conductivity detector (TCD) to detect gases formed during the combustion process. Each measurement involved approximately 5 mg of the sample, with the average of two analyses taken into account and calibration conducted with sulfanilamide.

### Bicinchoninic Acid Test

The principle of the bicinchoninic acid (BCA) assay is based on the formation of a Cu<sup>2+</sup>-protein complex under alkaline conditions, followed by the reduction of Cu<sup>2+</sup> to Cu<sup>1+</sup>. The fraction of reduced ions is proportional to the amount of protein. The procedure is easily carried out using a microplate reader and requires small volumes (10–25 μL) of protein sample. The necessary supplies were 96 microwell plates that were acquired from Thermo Scientific, USA, and an ELISA reader, called iMark (Bio-Rad, Italy). In every well, a final volume of 200 μL (150 μL BCA reagent + 50 μL samples) was added, and the mixture was incubated at 37 °C for 40 min, until the color developed. Using a bovine serum albumin

(BSA) concentration ranging from 200 to 1000 μg/mL, a standard curve was created during the test to compare the observed absorbance at 565 nm to the unknown protein concentrations.

### FE-SEM Analysis

For FE-SEM analyses, an FEI FEG-Quanta 450 instrument was utilized, with cellulose nanocrystals deposited on glass from a DMSO suspension at a concentration of 1 mg/L. Samples were coated with platinum before analysis, and the length of cellulose nanocrystals was measured using Image J 1.53e software, with standard deviation determined on the mean of over 30 measurements.

### ATR Analysis

ATR-FTIR spectra were acquired on a Thermo Scientific (mod. Is50) (Thermo Fischer Scientific, Madison, USA), equipped with an attenuated total reflectance (ATR) diamond cell for measurement in the 4000–4900 range. The attenuated total reflectance (ATR) for measurement in the 4000–650 cm<sup>-1</sup> region. For each sample, 16 scans with a resolution of 4 cm<sup>-1</sup> were collected. The ATR-FTIR spectra were recorded in triplicate. Spectra were reprocessed using Origin 2024 as the software.

### XRD Analysis

For XRD (X-ray diffraction) analyses, the measurements were performed using the X'Pert Pro MPD diffractometer from PANalytical company. The reflection mode and conventional geometry (Bragg-Brentano) were employed, utilizing a copper anode with characteristic Cu K<sub>α</sub> radiation and nickel filters to attempt monochromatization of the X-ray beam. A sample holder with zero background, specifically a single crystal of silicon specially cut to not produce a background signal, was utilized. The samples were mounted in a cavity within the sample holder, which was then spun at 0.25 Hz to ensure uniform irradiation. Only a square area (12 mm×8 mm) of the sample surface was irradiated, minimizing the exposure. The Segal method, a commonly used technique for estimating the crystallinity index of cellulose based on XRD data, was employed. This method involves comparing the intensity of crystalline peaks with the total intensity of both crystalline and amorphous peaks. The resulting ratio provides an estimate of the crystallinity index.<sup>[45]</sup>

### DLS and Zeta Potential

For DLS (dynamic light scattering) and zeta-potential measurements, a Zetasizer Nano ZS instrument from Malvern Panalytical was utilized. Standard 1 cm UV cuvettes were used for preparing DLS samples, while cuvettes equipped with two reduced-volume electrodes were employed for zeta-potential measurements. The measurements were conducted to analyze the size distribution and surface charge of the samples. Spectra obtained from these measurements were reprocessed using Origin 2024 software to extract relevant information about the samples' characteristics.

### Lysozyme Activity Test

The Lysozyme Detection Kit used for detecting the presence of lysozyme activity used *Micrococcus lysodeikticus* cells as the substrate. Lysozyme activity results in the lysis of the *Micrococcus lysodeikticus* cells in the time. The test allowed the calculation of the units/mL of enzyme by means of the following equation:

$$\frac{Ue}{mL} = \left( \frac{\Delta OD_{450}}{t_{test}} - \frac{\Delta OD_{450}}{t_{blank}} \right) / (df) (0.001) (0.03) \quad (1)$$

Where:

OD is the optical density

$\frac{\Delta OD_{450}}{t}$  is the slope of the curve calculated by the software Origin8 for each relevant experiment.

df = dilution factor

0.001 =  $\Delta OD_{450}$  as per the Unit Definition

0.03 = Volume (in milliliters) of enzyme solution

t is the time expressed in minutes.

Consequently, the solid units/mg equal to 3953700 for native lysozyme were calculated using the equation:

$$\frac{\text{units}}{\text{mg solid}} = \frac{\frac{\text{units}}{\text{mL enzyme}}}{\frac{\text{mg solid}}{\text{mL enzyme}}} \quad (2)$$

## Supporting Information Summary

Data on the characterization of lysozyme, nonspecifically immobilized lysozyme and DLS data of immobilized systems are given in the SI.

## Acknowledgements

This research was funded by the University of Pisa through the project "BIHO 2022-Bando Incentivi di Ateneo Horizon e Oltre" (Prot. n. 0048740/2022). LS acknowledges MUR (Ministero dell'Università e della Ricerca) for the project PON 2014–2020 (D.M. 1061/2021, CUP I59 J21017690008) entitled "Conversion of lignocellulosic biomass into cellulose fibers, lignin, and active biomolecules for the preparation of smart and sustainable coating for textiles of natural origin and similar flexible substrates". The authors thank CISUP (Center for Instrument Sharing of the University of Pisa) for the access to the FE-SEM facility. LGP2 is part of the LabEx Tec 21 (Investissements d'Avenir – grant agreement no ANR-11-LABX-0030) and of the PolyNat Carnot Institut (Investissements d'Avenir – grant agreement no ANR-11-CARN-030-01). Open Access publishing facilitated by Università degli Studi di Pisa, as part of the Wiley - CRUI-CARE agreement.

## Conflict of Interests

The authors declare no conflict of interest.

## Data Availability Statement

The data that support the findings of this study are available from the corresponding author upon reasonable request.

**Keywords:** Cellulose nanocrystals · Bioconjugation · Biocatalysis · Lysozyme · Enzymes immobilization

- [1] S. Gosh, J. K. Sinha, K. Vashisth, S. Han, R. Bhaskar, *Sustainability* **2023**, *15*, 10821.
- [2] M. Mujtaba, J. Lipponen, M. Ojanen, S. Puttonen, H. Vaitinen, *Sci. Total Environ.* **2022**, *851*, 158328.
- [3] S. Sun, X. Cao, R. Sun, *Bioresour. Technol.* **2016**, *199*, 49–58.
- [4] T. V. Patil, D. K. Patel, S. D. Dutta, K. Ganguly, T. S. Santra, K. Lim, *Bioact. Mater.* **2022**, *9*, 566–589.
- [5] TAPPI Standards: Regulations and Style Guidelines, Standard Terms and Their Definition for Cellulose Nanomaterial W 13021.
- [6] A. Dufresne, *Nanocellulose: From Nature to High Performance Tailored Materials*, De Gruyter, Berlin, Boston **2013**.
- [7] Y. Habibi, L. A. Lucia, O. J. Rojas, *Chem. Rev.* **2010**, *110*, 3479–3500.
- [8] A. Operamolla, C. Mazza, L. Capodici, F. Di Benedetto, L. Severini, M. Titubante, A. Martinelli, V. Castelvetro, L. Micheli, *ACS Appl. Mater. Interfaces* **2021**, *13*, 44972–44982.
- [9] S. Peng, Q. Luo, G. Zhou, X. Xu, *Polymers (Basel)*. **2021**, *24*, 3247.
- [10] L. Sillero, A. Morales, R. Fernández-Marín, F. Hernández-Ramos, I. Dávila, X. Erdocia, J. Labidi, *SCP* **2021**, *28*, 749–759.
- [11] U. Hanefeld, L. Gardossi, E. Magner, *Chem. Soc. Rev.* **2009**, *38*, 453468.
- [12] L. Spagnuolo, D. Beneventi, A. Dufresne, A. Operamolla, *ChemistrySelect* **2024**, *9*, e202401511.
- [13] S. V. Sancheti, P. R. Gogate, *Ultrason. Sonochem.* **2017**, *36*, 527–554.
- [14] A. Panja, V. Kumar, P. Jha, *Advances in Lignocellulosic Biofuel Production Systems, Woodhead*, **2023**, 129–141.
- [15] V. Noronha, C. H. M. Camargos, J. C. Jackson, A. G. Souza Fihlo, A. J. Paula, C. A. Rezendem, A. F. Faira, *ACS Sustainable Chem. Eng.* **2021**, *9*, 3203–3212.
- [16] S. Beluhan, K. Mihajlovski, B. Šantek, I. Šantek, *Energies* **2023**, *16*, 7003.
- [17] D. E. Cruz-Casas, C. N. Aguilar, J. A. Ascacio-Valdés, R. Rodríguez-Herrera, M. L. Chávez-González, A. C. Flores-gallegos, *Food Chem.* **2021**, *3*, 100047.
- [18] S. Cantone, V. Ferrario, L. Corici, C. Ebert, D. Fattor, P. Spizzo, L. Gardossi, *Chem. Soc. Rev.* **2013**, *42*, 6262–6276.
- [19] P. K. Robinson, *Essays Biochem.* **2015**, *59*, 1–41.
- [20] H. J. Kim, S. Park, S. Hee Kim, J. H. Kim, H. Yu, H. J. Kim, Y. Yang, E. Kan, Y. H. Kim, S. H. Lee, *J. Mol. Catal. B Enzyme* **2015**, *122*, 170–178 171.
- [21] A. Jebali, S. Hekmatimoghaddam, A. Behzadi, I. Rezapour, B. H. Mohammadi, T. Jasemizad, S. A. Yasini, M. J. Avadzadeh, A. Amiri, M. Soltani, Z. Rezaei, N. Sedighi, M. Seyfi, M. Rezaei, M. Sayadi, *Cellulose* **2013**, *20*, 2897–2907.
- [22] P. Mali, A. P. Sherje, *Carbohydr. Polym.* **2022**, *275*, 118668.
- [23] A. B. Rashid, M. E. Hoque, N. Kabir, F. F. Rifat, H. Ishrak, A. Alqahtani, M. E. H. Chowdhury, *Polymers (Basel)*. **2023**, *15*, 4070.
- [24] A. Abouhmad, T. Dishisha, M. A. Amin, R. Hatti-Kaul, *Biomacromolecules* **2017**, *18*, 1600–1608.
- [25] J. V. Edwards, N. T. Prevost, B. Condon, A. French, Q. Wu, *Cellulose* **2012**, *19*, 495–506.
- [26] P. Bayazidi, H. Almasi, A. K. Asl, *Int. J. Biol. Macromol.* **2018**, *107*, 2544–2551.
- [27] R. B. de Souza, U. I. Souza, S. Miranda, L. Lam, F. Santiago, M. D. Wasan, *RSC Adv.* **2015**, *9*, 34902–34911.
- [28] A. M. Weiss, N. Macke, Y. Zhang, C. Calvino, A. P. Esser-Kahn, S. J. Rowan, *ACS Biomater. Sci. Eng.* **2021**, *12*, 1450–1461.
- [29] X. Xing, Y. Han, Q. Jiang, Y. Sun, X. Wang, G. Qu, G. Sun, Y. Li, *Cellulose* **2021**, *28*, 4793–4805.
- [30] V. Incani, C. Danumah, Y. Boluk, *Cellulose* **2013**, *20*, 191–200.
- [31] A. Gennari, F. H. Mobayed, B. Da Rolt Nervis, E. V. Benvenuti, S. Nicolodi, N. Pesce da Silveira, G. Volpato, C. F. Volken de Souza, *Biomacromolecules* **2019**, *20*, 2315–2326.
- [32] S. Lin-Cao, Y.-M. Huang, X.-H. Li, P. Xu, H. Wu, N. Li, W.-Y. Lou, *Sci. Rep.* **2016**, *6*, 20420.
- [33] S.-L. Cao, H. Xu, X.-H. Li, W.-Y. Lou, M.-H. Zong, *ACS Sustainable Chem. Eng.* **2015**, *3*, 1589–1599.
- [34] M. S. Weiss, G. J. Palm, R. Hilgenfeld, *Acta Crystallogr.* **2000**, *D56*, 952–958.
- [35] M. S. Weiss, G. J. Palm, R. Hilgenfeld, *PDB Database*, **1999**, Entry - 1DPX. DOI: 10.2210/pdb1DPX/pdb.
- [36] N. Khorshidian, E. Khanniri, M. R. Koushki, S. Sohrabvandi, M. Yousefi, *Front. Nutr. Sci.* **2022**, *9*, 833618.
- [37] A. Bergamo, G. Sava, *Molecules* **2024**, *29*, 652.



- [38] S. Venkataramani, J. Truntzer, D. R. Coleman, *J. Pharmacy Bioallied Sci.* **2013**, *5*, 148–153.
- [39] N. Nawaz, S. Wen, F. Wang, S. Nawaz, J. Raza, M. Iftikhar, M. Usman, *Molecules* **2022**, *27*, 6305.
- [40] P. Ferraboschi, S. Ciceri, P. Grisenti, *Antibiotics* **2021**, *14* (10), 1534.
- [41] A. Operamolla, S. Casalini, D. Console, L. Capodiecì, F. Di Benedetto, G. Valerio Bianco, F. Babudri, *Soft Matter* **2018**, *14*, 7390–7400.
- [42] D. Neagu, *Anal. Bioanal. Chem.* **2006**, *385*, 1068–1074.
- [43] H. Fukuzumi, T. Saito, Y. Okita, A. Isogai, *Prog. Polym. Sci.* **2010**, *959*, 1502–1508.
- [44] R. D'Orsi, V. C. Canale, R. Cancelliere, O. Hassan Omar, C. Mazzuca, L. Micheli, A. Operamolla, *Eur. J. Org. Chem.* **2023**, *26*, e202201457.
- [45] L. Segal, J. J. Creely, *An. Text. Res. J.* **1959**, *29*, 786–794.
- [46] F. A. Quijoch, *Biochemistry (Mosc.)* **1966**, *5*, 4062–4076.
- [47] S. Kongruang, M. Joo Han, C. Isela, G. Breton, M. H. Penner, *Appl. Biochem. Biotechnol.* **2004**, *113–116*, 213–231.

---

Manuscript received: June 4, 2024

Accepted manuscript online: August 14, 2024

Version of record online: October 16, 2024